Korean J. Chem. Eng., 40(8), 1954-1962 (2023)
DOI: 10.1007/s11814-023-1473-4

pISSN: 0256-1115
eISSN: 1975-7220

Thermoresponsive, dually cross-linked elastin-like-polypeptide (ELP) micelle hydrogel with recovery properties

Jongsoo Choi, Moon-Chul Ryu, Jae Jung Kim, Soo-Hyung Choi, and Jong-In Won†

Department of Chemical Engineering, Hongik University, Seoul 04066, Korea
(*Received 9 March 2023 • Revised 12 April 2023 • Accepted 17 April 2023*)

Abstract−Thermoresponsive protein-based hydrogels have been widely used due to their high potential in biomedical fields. Elastin-like polypeptides (ELPs) are one of the proteins that show lower critical solution temperature (LCST) behavior, resulting in self-assembly above critical micellular temperature (CMT). Here, we utilized ABC-type blocky ELPs to form hydrogels by introducing cross-linking sites, resulting in good mechanical properties. The hydrogels showed temperature-dependent viscoelasticity due to their structure change. Also, the recovery process of ELP-based hydrogels after large deformation is significantly dependent on the types of cross-linking (*i.e.*, ionic, covalent, or ionic-covalent hybrid).

Keywords: Elastin-like Polypeptides (ELPs), ELP-based Hydrogel, Block Copolymer, Cross-linking

INTRODUCTION

Advances in molecular biology allow for the design of engineered recombinant proteins. The hydrogel formed by such designed protein has been widely used in various fields, such as drug delivery, tissue engineering, and biosensors [1-7]. While such protein/polypeptide-based hydrogel has advantages in terms of biocompatibility and low cytotoxicity [8-10], it is limited in practice due to the weak mechanical properties. Recently, the self-assembly behavior of biopolymers has been extensively explored. ELP is one of the synthetic polypeptides that shows self-assembly behavior. The amino acid sequence of ELP is derived from native tropoelastin [11] composed of Val-Pro-Gly-Xaa-Gly (VPGXG) repeating units where Xaa is a guest residue, which can be any amino acid except Pro [12]. ELPs undergo a reversible phase transition between soluble and insoluble phases at a lower critical solution temperature (LCST). When ELPs are composed of amphiphilic blocks, they self-assemble into micelles above critical micelle temperature (CMT) [13,14]. Described thermal behaviors (*i.e.*, LCST, CMT) of ELPs are dependent on pH, molecular weight, concentration, and of the guest residue (Xaa) [13,15,16]. Recently, hydrogels with two types of cross-linking (*i.e.*, dually cross-linked or hybrid cross-linked hydrogel) were explored to improve their toughness, stretchability, recovery properties, and self-healing properties [17,18]. Interpenetrating polymer network would be the most prevalent example. Two distinct polymer networks were interpenetrated while each polymer network had its own cross-linking site. For instance, an ionically cross-linked alginate network and a chemically cross-linked polyacrylamide network were interpenetrated to form an alginate/polyacrylamide hydrogel with great stretchability [19]. The dually cross-linked hydrogel also can be formed by having two distinct cross-linking sites in a single polymer network [20]. Another approach is to make a covalently cross-linked polymer network with micelles which serve as a physical cross-linking site [21]. In these dually cross-linked hydrogels, one cross-linking site dissipates the stress generated over the deformation process, while another cross-linking site tends to preserve the initial state of the network.

In this study, we utilized the self-assembly behavior of a synthetic triblock ELP, $V_{36}C_{36}$kzinc (V_{36}: hydrophobic block, C_{36}: hydrophilic block, and kzinc: cross-linking block) to form a dually cross-linked hydrogel. Self-assembled ELP micelles were formed through aggregation of the hydrophobic block of ELP, and serve as the first cross-linking site when it forms the hydrogel later. Above the critical temperature, the self-assembly behavior of ELP was confirmed by UV-visible spectrophotometry, dynamic light scattering (DLS), ^{1}H NMR spectrometry, and transmission electron microscopy (TEM). Next, the hydrogel was formed by self-assembled ELP micelle using cross-linking agents. Depending on the type of cross-linking, we classified the hydrogels into three types: I-gel formed by Zn^{2+} ionic cross-linking, C-gel formed by tetrakis(hydroxymethyl)phosphonium chloride (THPC)-based covalent cross-linking, and H-gel formed by both ionic and covalent cross-linking. We measured the viscoelastic properties of these hydrogels by rheometer and validated that reversible sol-gel transition was induced by changing the temperature. The types of cross-linking (i.e., ionic, covalent, or ionic-covalent hybrid) resulted in a difference in the recovery rate. We envision that these distinct types of hydrogels can be used in a wide range of biomedical applications, such as drug delivery system, tissue engineering, and biosensors.

MATERIALS AND METHODS

1. Cloning of the Triblock ELP Genes

Primers (Fig. 1; Bioneer, Korea) designed to obtain the V_3 gene (three repeats encoding VPGVGVPGVG), C_3 gene (three repeats encoding VPGAGVPGGG), and kzinc gene (VPGKGHEDGH-

†To whom correspondence should be addressed.
E-mail: jiwon@hongik.ac.kr

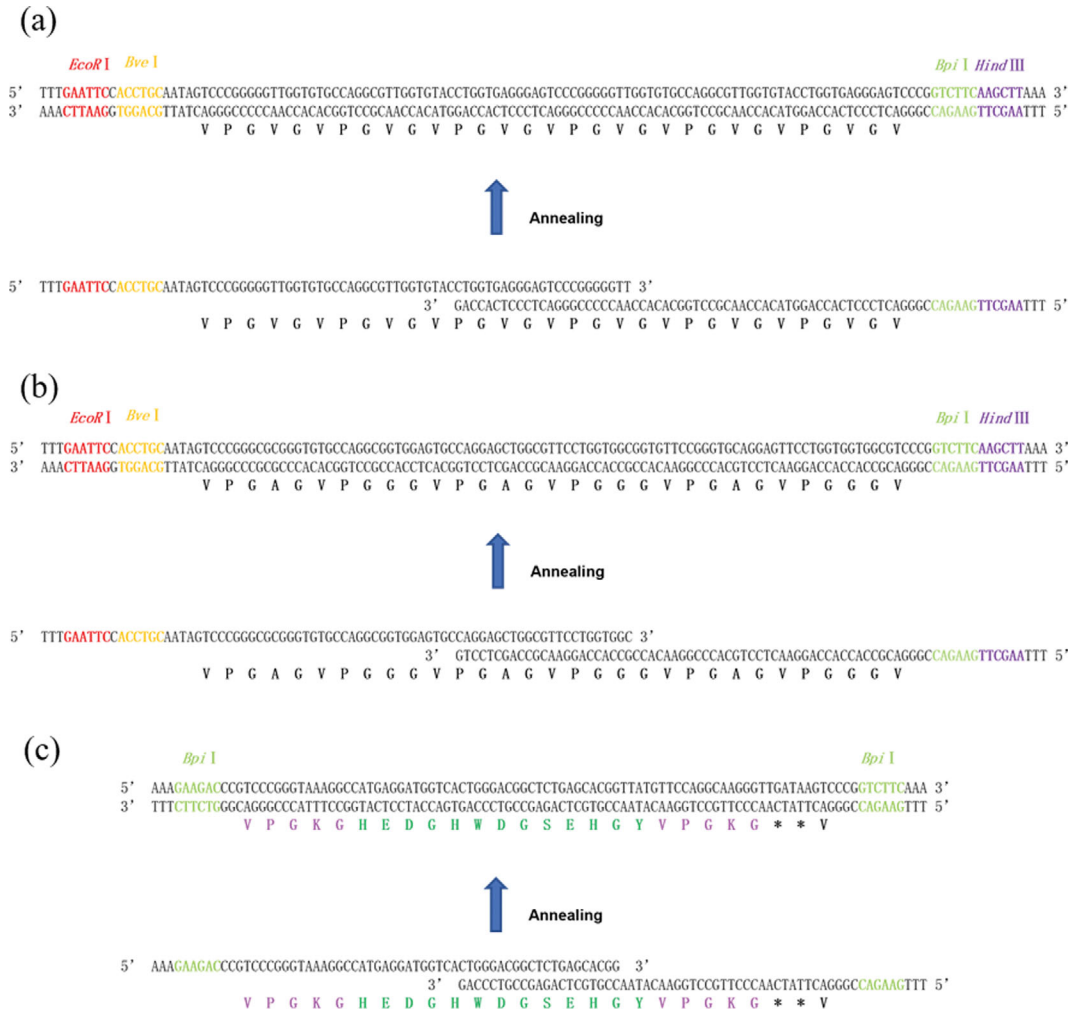

Fig. 1. Formation of ELP monomer and cross-linked site genes. DNA and corresponding polypeptide sequences of (a) ELP monomer gene (V_3 block) (b) ELP monomer gene (C_3 block) (c) Cross-linked site gene (kzinc block).

WDGSEHGYVPGKG) were prepared and cloned into pUC19 vector (Novagen, USA) by treating V_3 and C_3 genes with *Eco*RI and *Hind*III endonucleases (Enzynomics, Korea). Cloned ELP monomer genes were multimerized by recursive directional ligation through the plasmid reconstruction (Pre-RDL) method [22] using two sets of restriction enzymes, *Bsa*I/ *Bve*I and *Bsa*I/ *Bpi*I (*Bsa*I, Enzynomics, Korea; *Bve*I and *Bpi*I, Thermo Fisher Scientific, USA). As a result, V_{36} and C_{36} genes were produced. Next, V_{36} and C_{36} genes, digested with *Bsa*I/*Bpi*I and *Bsa*I/*Bve*I, were ligated to generate the diblock ELP gene. Subsequently, $V_{36}C_{36}$ and kzinc genes, digested with *Bpi*I, were ligated to generate the triblock ELP gene. DNA sequencing was performed to verify the preparation of the desired sequence. After the target gene was treated with *Bpi*I and *Bve*I restriction enzymes, it was transferred to the pET32a(+) vector [23] and transformed into BLR(DE3) (Novagen, USA). To identify the size, cloned genes were analyzed by 1% agarose gel electrophoresis using *Nco*I (Enzynomics, Korea) and *Hind*III digestion. DNA sequence analyses of these genes were performed to verify the sequence.

2. Protein Expression and Purification

Transformed cells were cultured in Terrific Broth (TB, 3 L) supplemented with ampicillin (70 μg/ml). Cells were incubated at 37 °C until the OD_{600} reached 0.6-0.8. Then, protein synthesis was induced by 0.1 mM of isopropyl-*β*-D-thiogalactoside (IPTG; Glentham Life Sciences, UK), and the temperature was switched to 30 °C. After a 14-h culture, the cells were harvested by centrifugation at 6,500 ×g for 15 min at 4 °C, and resuspended in 200 mL of phosphate-buffered saline (137 mM NaCl, 2.7 mM KCl, 10 mM Na_2HPO_4. 1.8 mM KH_2PO_4, pH 7.4). The resuspended cells were sonicated for 3 min at pulses of 10 s ON/30 s OFF to prevent the overheating of the solution. Cell lysates were centrifuged at 12,000 ×g for 1 h at 4 °C to remove insoluble cell debris, and NaCl was added to the lysates to trigger the inverse transition. $V_{36}C_{36}$kzinc was purified using inverse transition cycling (ITC) method [24] and analyzed by 12% sodium dodecyl sulfate-polyacrylamide gel electrophoresis (SDS-PAGE). After analysis, purified $V_{36}C_{36}$kzinc was dialyzed sufficiently, then freeze-dried to obtain the protein in powder form. Since the pET32a vector is designed to express Trx-tag, the tag was required to be removed through CNBr treatment (Sigma-Aldrich, USA). After CNBr treatment, ITC purification was repeated three times. The purity of the protein was confirmed by matrix-assisted laser

desorption ionization time-of-flight (MALDI-TOF) because there were few stainable amino acid sequences.

3. Characterization of ELPs

Thermal behavior of the triblock copolymer was evaluated by measuring OD_{350} at a protein concentration of 50 μM. Cary 100 Bio UV-visible spectrophotometer with a temperature scanning function (Agilent Technologies, USA) was used to measure OD_{350}. Temperature changed from 10 °C to 70 °C at a rate of 1 °C/min. DLS was used to validate its thermal behavior. While changing the temperature from 10 °C to 60 °C, self-assembly behavior of $V_{36}C_{36}$kzinc (50 μM) was analyzed using DLS (ZEN1690, Malvern, UK) with λ=532 nm and a scattering angle of 90°. The morphology of self-assembled ELPs was observed by TEM. 50 μM of ELPs in PBS buffer was placed on a carbon support film/copper grid (Sigma-Aldrich, USA). The sample was added to the grid one more time, followed by the application of 1% K-PTA (phosphotungstic acid, adjusted to pH 5.5 with KOH) solution. The excess water was removed and the grids were dried in the oven. The samples were observed using a JEM-2100PLUS (JEOL, Japan) at 200 kV. ^{1}H NMR was performed in D_2O solution using Avance III 500 MHz (Bruker, Germany) spectrometer. We waited for 10 min before measurement to have samples reach equilibration at the corresponding temperature.

4. Hydrogel Preparation

ELPs were dissolved in PBS buffer at a target concentration. Either zinc ion, THPC, or a mixture of zinc ion and THPC were added to the solution. I-gel was made by adding zinc sulfate to 10 or 20 w/v% ELP solution. The molar ratio of the zinc-binding site to zinc ion was 0.13-1. C-gel was made by adding THPC to 10 w/v% ELP solution. The molar ratio of the THPC binding site to THPC was 4. H-gel was made by adding zinc sulfate first and THPC about 1 h later. Compared to the I-gel and C-gel, H-gel was made by adding half the zinc sulfate and THPC. I-gel and C-gel were designed

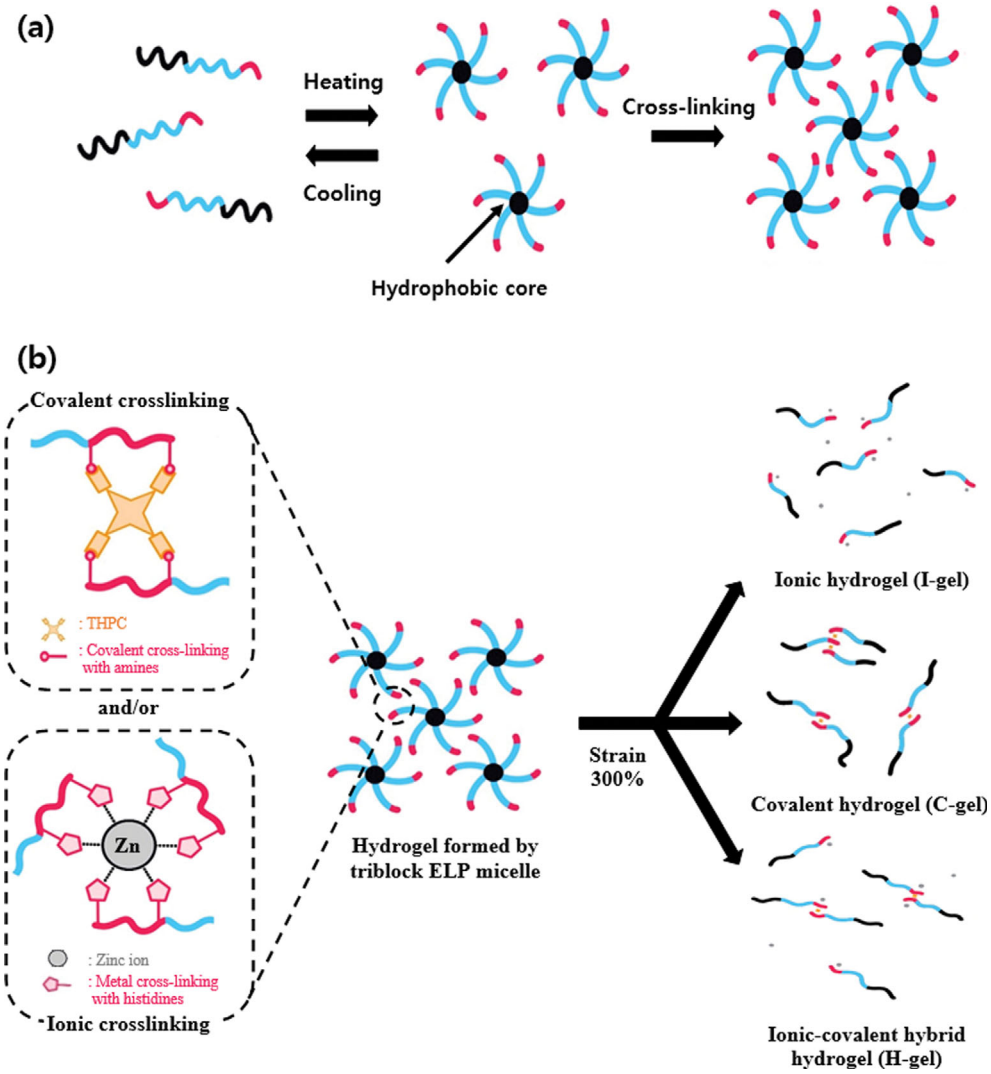

Fig. 2. Hydrogels formed by triblock ELP, $V_{36}C_{36}$kzinc. (a) Thermoresponsive micelle formation and cross-linking-based hydrogel formation. Micelle is formed by hydrophobic interaction at a temperature above CMT. (b) Covalent cross-linking is formed by adding THPC to ELPs, and ionic cross-linking is formed by adding zinc ions. Depending on the type of cross-linking, ELP hydrogel shows distinct physical properties.

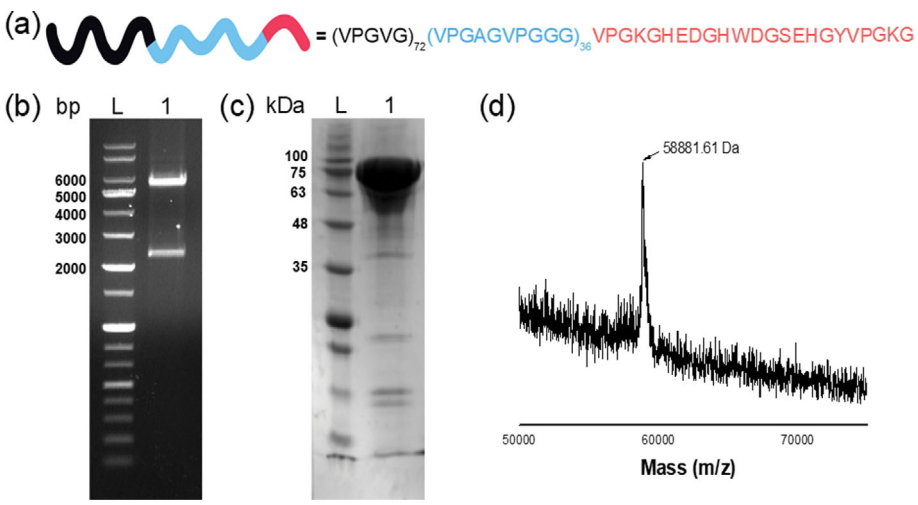

Fig. 3. Design and characterization of triblock ELP ($V_{36}C_{36}$kzinc). (a) Amino acid sequence of $V_{36}C_{36}$kzinc. (b) Electrophoresis of $V_{36}C_{36}$kzinc gene (2,229 bp). (c) Coomassie blue staining of the expressed $V_{36}C_{36}$kzinc (79 kDa). (d) MALDI-TOF mass spectrum of $V_{36}C_{36}$kzinc (58,881 Da).

to have saturated ionic/covalent cross-linking while H-gel had both covalent and ionic cross-linking, which were half saturated, at the same time. Then, the solution was vigorously vortexed for 1 min at 40 °C. Formed hydrogels were kept in a sealed vial at 40 °C for 24 h and centrifuged for a short time to remove air bubbles before measuring the mechanical properties.

5. Characterization of ELP Hydrogels

Rheological properties were measured by an MCR302 rheometer (Anton Paar) equipped with a parallel plate geometry of 25 mm diameter. Hydrogels were loaded on a lower plate, and an upper plate was lowered to make a 0.400 mm gap between plates. The plate temperature was controlled by a Peltier element, and an evaporation blocker was used to minimize water evaporation. Prior to all measurements, time sweep measurements were performed for at least 30 min to reach the equilibrium. Strain sweep measurements were performed to determine the linear viscoelastic regime. Temperature sweep measurements were conducted at an angular frequency of 1 Hz (6.28 rad/s) and a strain of 0.1% while the temperature was varied between 20 and 45 °C with a ramping rate of 1 °C/min. The gelation temperature was determined as a temperature where the storage modulus and loss modulus were crossed. Frequency sweep measurements were performed with a frequency range between 0.1 and 100 rad/s at 40 °C. Cyclic strain measurements were performed upon periodic strain between 0.1 and 300% and at 40 °C. Strain jump measurements were performed with immediate strain change from 300% to 0.1% at 40 °C.

RESULTS AND DISCUSSION

1. Design and Purification of Triblock ELP

In this study, we synthesized triblock ELP, $V_{36}C_{36}$kzinc, to form hydrogels with distinct cross-linking types (Fig. 2). $V_{36}C_{36}$kzinc consists of three blocks. V_{36} and C_{36} refer to a hydrophobic block, $(VPGVGVPGVG)_{36}$, and a hydrophilic block, $(VPGAGVPGGG)_{36}$, respectively. Because ELPs form a hydrogel through cross-linking, $V_{36}C_{36}$kzinc is designed to have a third block, a cross-linking block, at the hydrophilic terminus. The cross-linking block, kzinc, is composed of two parts: 1) ionic cross-linking, and 2) covalent cross-linking sites. For the first part, HEDGHWDGSEHGY peptide was chosen because it has an amino acid sequence similar to the consensus zinc-binding sequence of matrix metalloproteinases [25,26]. For the second part, VPGKG was chosen because it can be covalently crosslinked by adding THPC [27]. By adding the second part at both sides of the first part, we designed the sequence of the cross-linking block, VPGKGHEDGHWDGSEHGYVPGKG (Fig. 3(a)).

The cloned gene was transferred from the pUC19 vector to the pET32a(+) vector, which is subjected to restriction enzyme treatment with *Nco*I and *Hind*III. To validate the gene transfer, 1% agarose gel electrophoresis was tested (Fig. 3(b)). The recombinant plasmid was transformed into BL21(DE3), and expressed protein was identified by SDS-PAGE (Fig. 3(c)). However, as can be seen, it was difficult to confirm expressed $V_{36}C_{36}$kzinc on SDS-PAGE after CNBr treatment, which is required to remove the Trx-tag, a characteristic of the pet32a(+) vector. Therefore, after three repeats of inverse transition cycling (ITC) purification, expressed $V_{36}C_{36}$kzinc was confirmed using MALDI-TOF mass spectroscopy (Fig. 3(d)).

2. Self-assembly of Triblock ELP

The LCST phase behavior of $V_{36}C_{36}$kzinc was examined at different concentrations. At CMT, block copolymer forms the micelle because the hydrophobic blocks aggregate to form a spherical core. Such CMT is defined as the point at which optical density at 350 nm (OD_{350}) starts to increase above the baseline [28]. Turbidity of aqueous $V_{36}C_{36}$kzinc solution (concentration=25, 50, 100, or 200 μM) is plotted as a function of temperature (Fig. 4(a)). At 50 μM of ELPs, CMT was estimated as 37 °C. When salt was added to the solution, CMT decreased to 34, 32, and 25 °C at 0.25, 0.5, and 1 M of salt, respectively. Inverse transition temperature (T_t) is the temperature at which soluble ELPs aggregate in the solution. At T_t, unlike the CMT, not only hydrophobic blocks but also hydrophilic blocks participate in the aggregation process. T_t is defined as the temperature at the maximum point of turbidity gradient [16]. In the absence of salt, T_t was observed in the given temperature

range (15-70 °C). Meanwhile, when salt concentration increased to 0.25, 0.5, and 1 M, T_t was observed and decreased to 65, 60, and 55 °C (Fig. 4(b)).

DLS was used to confirm the self-assembly of $V_{36}C_{36}$kzinc into micelles. $V_{36}C_{36}$kzinc's hydrodynamic radius (R_h) was measured as 9 nm below CMT, and increased to 38 nm above CMT (Fig. 4(c)). This result is consistent with the previous study of micelles formation of amphiphilic ELP [29]. Morphology of self-assembled $V_{36}C_{36}$kzinc was analyzed using transmission electron microscopy (TEM). TEM image showed that $V_{36}C_{36}$kzinc formed a spherical micelle above CMT, and it had a radius close to that measured by DLS (Fig. 4(d)).

We investigated the structure of self-assembled $V_{36}C_{36}$kzinc by ^{1}H NMR. In previous studies, the structure of block copolymer micelle was explored by calculating the intensity change of two peaks before and after micelle formation: peak assigned to hydrophobic block, and hydrophilic block [30,31]. By adopting this approach, we took ^{1}H NMR of $V_{36}C_{36}$kzinc in pure D_2O at two temperatures: 20 °C (below CMT) and 50 °C (above CMT). Based on the previous studies [32,33], peak assignments to the chemical structure of $V_{36}C_{36}$kzinc are shown in Fig. 5(a). When $V_{36}C_{36}$kzinc is self-assembled into micelle, valine in the hydrophobic block (red-shaded) moves to the core, while alanine in the hydrophilic block (green-shaded) and lysine in the cross-linking block (yellow-shaded) move to the corona. Thus, the intensity change of these three peaks indicates the presence of micelles with a hydrophobic core and hydrophilic corona. As expected, the relative intensity of the hydrophobic block to both hydrophilic and cross-linking blocks decreased as the temperature changed from 20 °C to 50 °C (Fig. 5(b)). After increasing the temperature, all signals were shifted to the downfield because of thermally induced dehydration [34-36].

To further explore the change in the heating process, we calculated the *p*-fraction, the fraction of phase-separated units in globular structures. *p*-Fraction was calculated from the integrated intensity of the resonance peaks in ^{1}H NMR spectrum using Eq. (1) [37,38]:

$$p = 1 - \frac{I(T)}{I(T_0)} \quad (1)$$

I(T) is the integrated intensity of the signal at 50 °C, and $I(T_0)$ is the integrated intensity of the same signal at 20 °C. It is noted that all peak areas were normalized using the peak corresponding to lysine because the lysine-containing block is presumably soluble regardless of temperature. When *p*-fraction is close to 1, the signal

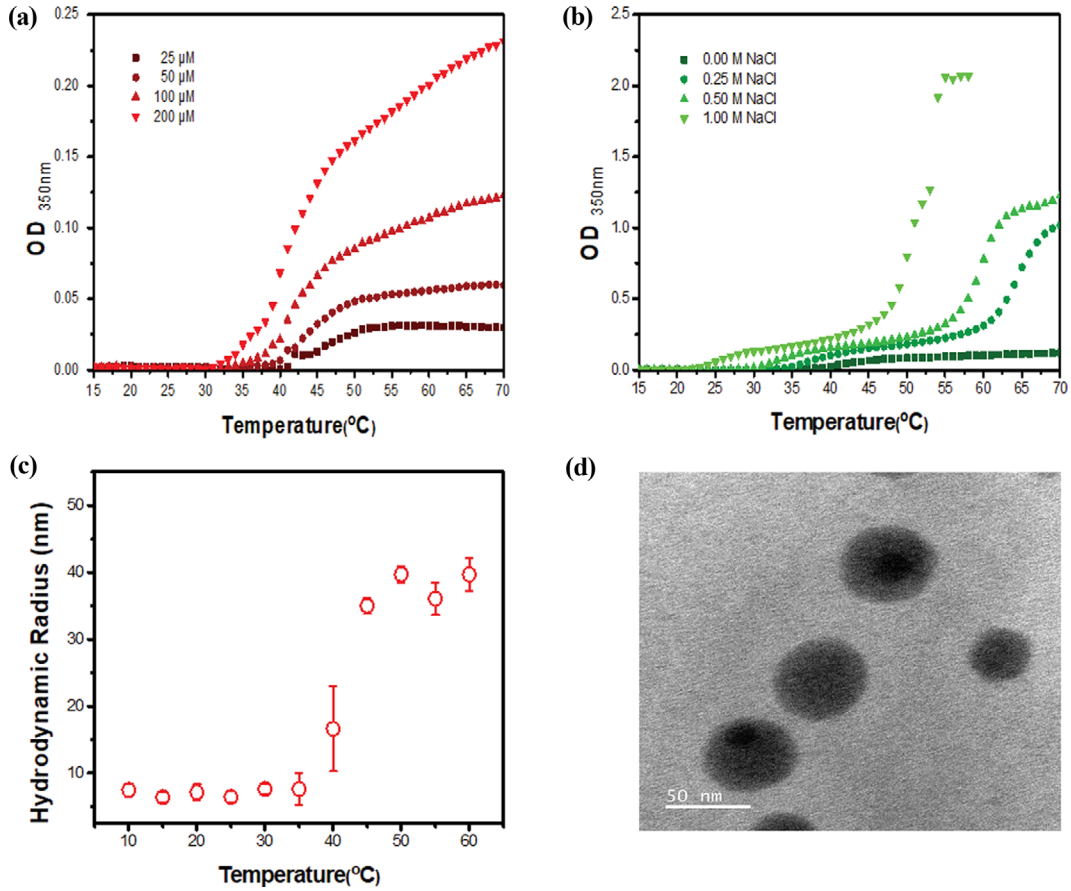

Fig. 4. Thermally triggered self-assembly of $V_{36}C_{36}$kzinc. (a) Turbidity profiles of $V_{36}C_{36}$kzinc solution (25, 50, 100, and 200 μM) as a function of temperature. (b) Turbidity profiles of 100 μM $V_{36}C_{36}$kzinc solution in various NaCl concentrations (0 to 1.0 M). Optical density was measured in triplicate by UV-Vis spectrometer (λ=350 nm). Representative data of three replicates is shown in the plot. (c) Hydrodynamic radius (R_h) of $V_{36}C_{36}$kzinc (100 μM) as a function of temperature. R_h was measured in triplicate by DLS. The average and standard deviation were shown in the plot. (d) TEM image of the self-assembled $V_{36}C_{36}$kzinc. $V_{36}C_{36}$kzinc is assembled into spherical micelle. The average size of micelles in the TEM image was 28 nm.

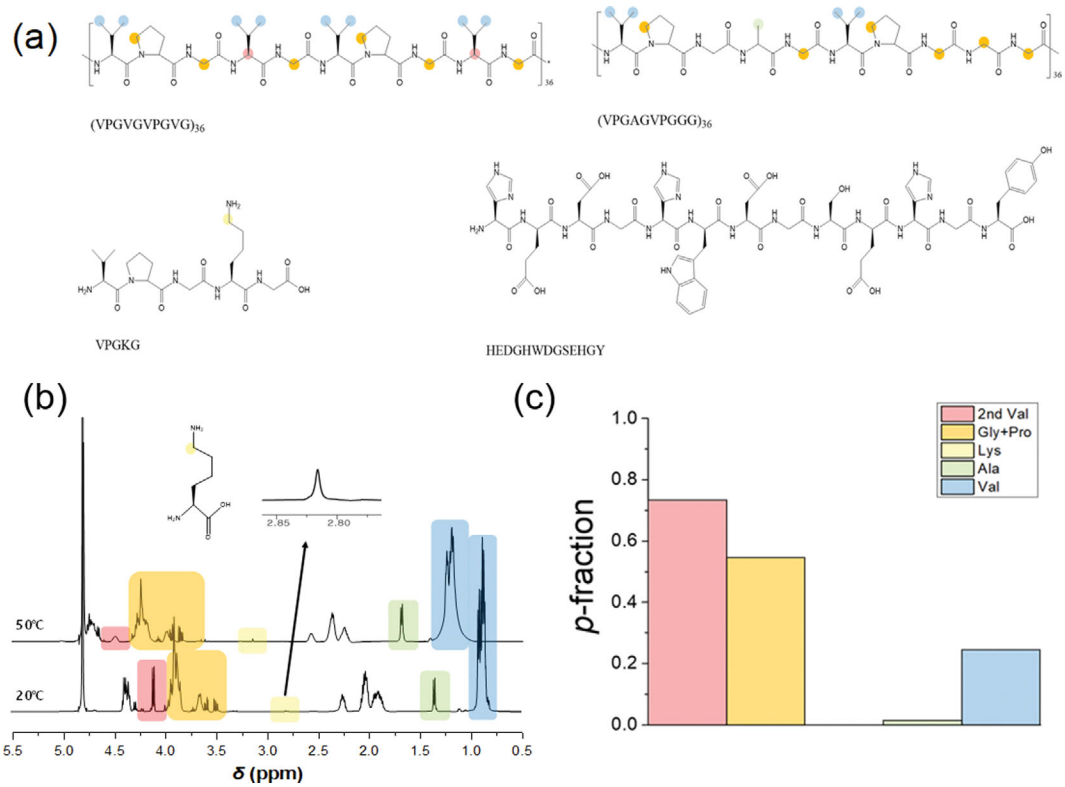

Fig. 5. ^{1}H NMR of $V_{36}C_{36}$kzinc before and after self-assembly. (a) Chemical structure of repeating unites. Shaded spots in the chemical structure correspond to ^{1}H NMR peak in (b). (b) ^{1}H NMR spectrum of $V_{36}C_{36}$kzinc dissolved in pure D_2O at 20 °C and 50 °C. NMR peaks are shown without normalization. ^{1}H signal of α-carbon of the second valine in the hydrophobic block is shaded in red. ^{1}H signal of β-carbon of alanine in the hydrophilic block is shaded in green. ^{1}H signal of ε-carbon of lysine in the cross-linking site is shaded in yellow. ^{1}H signals of α-carbon of glycine and δ-carbon of proline are shaded in orange. ^{1}H signal of γ-carbon of valine is shaded in blue. After changing the temperature from 20 °C to 50 °C, the relative intensity of the red-shaded signal to yellow and green decreased, representing the formation of the hydrophobic core of micelles. (c) *p*-fraction of ^{1}H NMR peaks. When calculating *p*-fraction, NMR peaks were normalized based on the lysine because the lysine-containing block would be soluble at both 20 and 50 °C.

disappears after self-assembly. On the other hand, when *p*-fraction is close to 0, the signal does not change after the temperature increases. *p*-fraction is summarized in Fig. 5(c). *p*-Fraction of α-carbon of the second valine in the hydrophobic block was 0.73. This fact implies that the hydrophobic block moved to the core at 50 °C. On the other hand, *p*-fraction of β-carbon of alanine in the hydrophilic block was 0.01. This fact implies that hydrophilic block moved to the corona at 50 °C. Meanwhile, signals corresponding to the residue, which exist in both hydrophobic and hydrophilic blocks, have the intermediate *p*-fraction. *p*-fraction of α-carbon of glycine and δ-carbon of proline was 0.55 while one of γ-carbon of valine was 0.24.

3. Formation of ELP Hydrogel

We utilized the cross-linking site in the corona of self-assembled $V_{36}C_{36}$kzinc micelles to form a hydrogel. Depending on types of cross-linking, we classified the type of hydrogels: ionic hydrogel (I-gel) formed by ionic cross-linking, covalent hydrogel (C-gel) formed by covalent cross-linking, and ionic-covalent hybrid gel (H-gel) formed by both ionic and covalent cross-linking.

We tested the activity of ionic and covalent cross-linking sites separately. A small amount of zinc sulfate or THPC was added to $V_{36}C_{36}$kzinc solution (100 μM) at 25 °C and 50 °C. Then, after waiting for 30 minutes for the equilibrium, we measured OD_{350} (Fig. 6(a), (b)). When self-assembled ELPs formed the hydrogel, the solution became opaque, increasing OD_{350}. As can be seen, OD_{350} increased when two requirements were satisfied at the same time: 1) $V_{36}C_{36}$kzinc formed the micelle at 50 °C, and 2) cross-linking was formed by adding either Zn^{2+} or THPC. This result implies that cross-linking blocks in the corona are active as we designed.

As can be seen in OD_{350} results, hydrogels were formed only when the hydrophobic block formed a core of micelles and the corona of micelles was cross-linked. The reversible transition of hydrogel was achieved by not satisfying one of requirements. We validated this concept with I-gel. When Zn^{2+} was added to $V_{36}C_{36}$kzinc solution at low temperature, the solution was still translucent (Fig. 6(c)). Although cross-linking blocks were cross-linked, hydrophobic blocks were not aggregated, resulting in a clear solution without forming a hydrogel. As the temperature increased to 50 °C higher than CMT, a hydrophobic block formed the core of the micelle, and the corona was still ionically cross-linked, forming opaque I-gel. When the temperature decreased to 25 °C lower than CMT, the core of micelles became free hydrophobic blocks, and a phase transition into the solution occurred. We achieved such thermally induced phase transition reversibly.

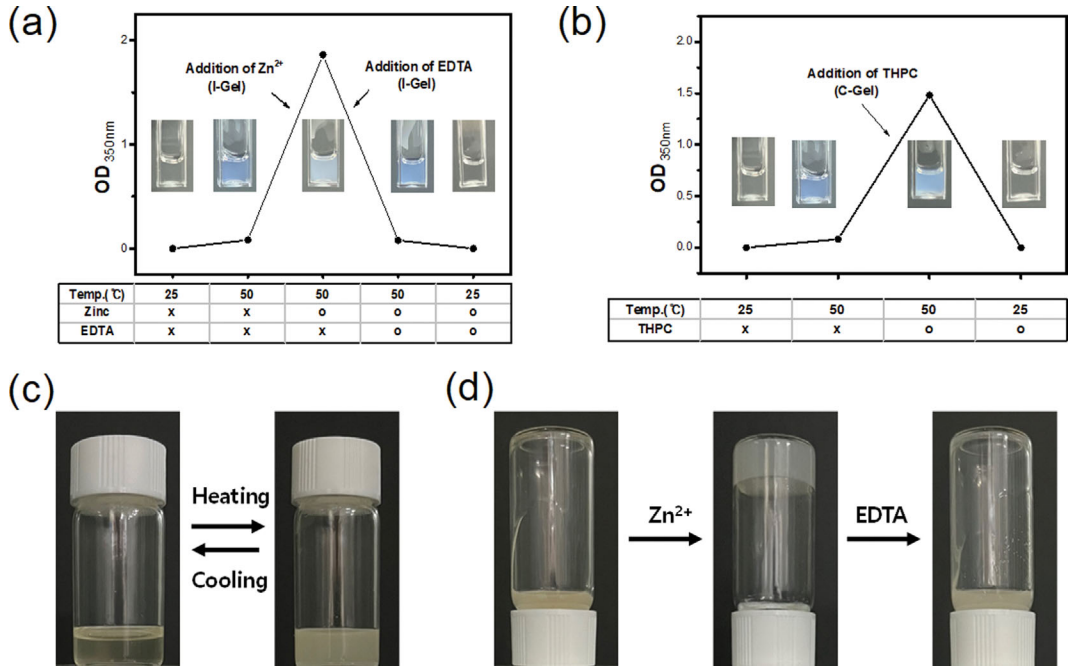

Fig. 6. A formation of the hydrogel by self-assembled $V_{36}C_{36}$kzinc micelles. (a), (b) Optical density (λ=350 nm) of $V_{36}C_{36}$kzinc solution (100 μM) after adding zinc ion (a) or THPC (b). High opacity indicated that hydrogels were formed. When EDTA was added to the solution with zinc ion, the hydrogel was not formed because zinc ion was chelated by EDTA. (c) The thermally induced reversible transition between ionic hydrogel (I-gel) and solution. (d) Phase transition of I-gel induced by adding zinc ion and EDTA. As EDTA chelated the zinc ion, ionic cross-linking was lost, resulting in a phase transition into the solution.

As we induced the phase transition by tuning the status of hydrophobic core, the phase transition was also controlled by the status of ionic cross-linking (Fig. 6(d)). When Zn^{2+} was added into ELP solution at 50 °C, I-gel was formed. Phase transition to solution was induced by adding EDTA. This is because EDTA chelated zinc ions and break the ionic cross-linking of I-gel.

4. Viscoelasticity of ELP Hydrogels

We successfully formed three types of hydrogels (*i.e.*, I-gel, C-gel, and H-gel). Fig. 7(a) shows the strain sweep of the storage modulus (G′) and loss modulus (G″) for three hydrogels. For all hydrogels, both G′ and G″ were constant at strains below 0.4%. Then, there was a sharp decline in G′ and G″ at strains above 0.4%. Therefore, the linear viscoelastic regime, in which G′ and G″ were independent of the strain, was confirmed to be 0.4% or less.

Subsequently, frequency sweep measurements were performed at a strain of 0.1%. Fig. 7(b) shows the plateau modulus of each hydrogel at 20 °C, 30 °C, and 40 °C. The plateau moduli (G_N) were obtained using the constant value of G′ at high frequency; the number density of elastically active chains (v) could be calculated by Eq. (2) [8,39]:

$$v = \frac{G_N}{k_B T} \quad (2)$$

where k_B is the Boltzmann constant, and T is the temperature. All hydrogels showed similar G_N values at 40 °C. This fact implies that a similar number of cross-linking was formed at 40 °C. Between different types of hydrogels, there is no difference in the hydrophobic core of self-assembled micelles, having no effect on v. Thus, v solely depends on the density of cross-linking between the corona of micelles. Because the cross-linking site is designed to be at the end of the corona, the cross-linking density is determined by the amount of Zn^{2+} and THPC added.

Next, we measured the linear rheological properties of hydrogels at 40 °C. G′ and G″ of the H-gel at 10 and 20 wt% were measured using the frequency sweep (Fig. 7(c)). G′ was larger than G″, and both G′ and G″ were independent of frequency across the experimental range. These results also validate the formation of hydrogel, a cross-linked polymer network.

As shown in Fig. 6(c), sol-gel transition could be reversibly induced by changing the temperature because of the CMT behavior of $V_{36}C_{36}$kzinc. We validated such sol-gel transition of H-gel through temperature sweep measurement (Fig. 7(d)). At low temperature, G″ was larger than G′. As the temperature increased, a crossover occurred: G′ exceeded G″. In addition, the modulus increased by ~10^4 times. This crossover temperature represents CMT, which was ~32.5 °C.

5. Recovery Properties of ELP Hydrogels

We tested the recovery property of $V_{36}C_{36}$kzinc hydrogels. The cyclic strain of $V_{36}C_{36}$kzinc hydrogel was measured upon periodic strain between 0.01-300% (Fig. 8(a)). All three hydrogels (I-gel, C-gel, and H-gel) showed a liquid-like behavior at high strain followed by immediate recovery to a solid-like behavior at low strain. All hydrogels recovered according to the change in periodic strain. In the beginning of measurement, they had a G′ of ~2.0×10^6 Pa at low strain (0-100 s). Then, they showed the difference in G′ in recovery period (200-300 s, 400-500 s, and 600-700 s). At high strain,

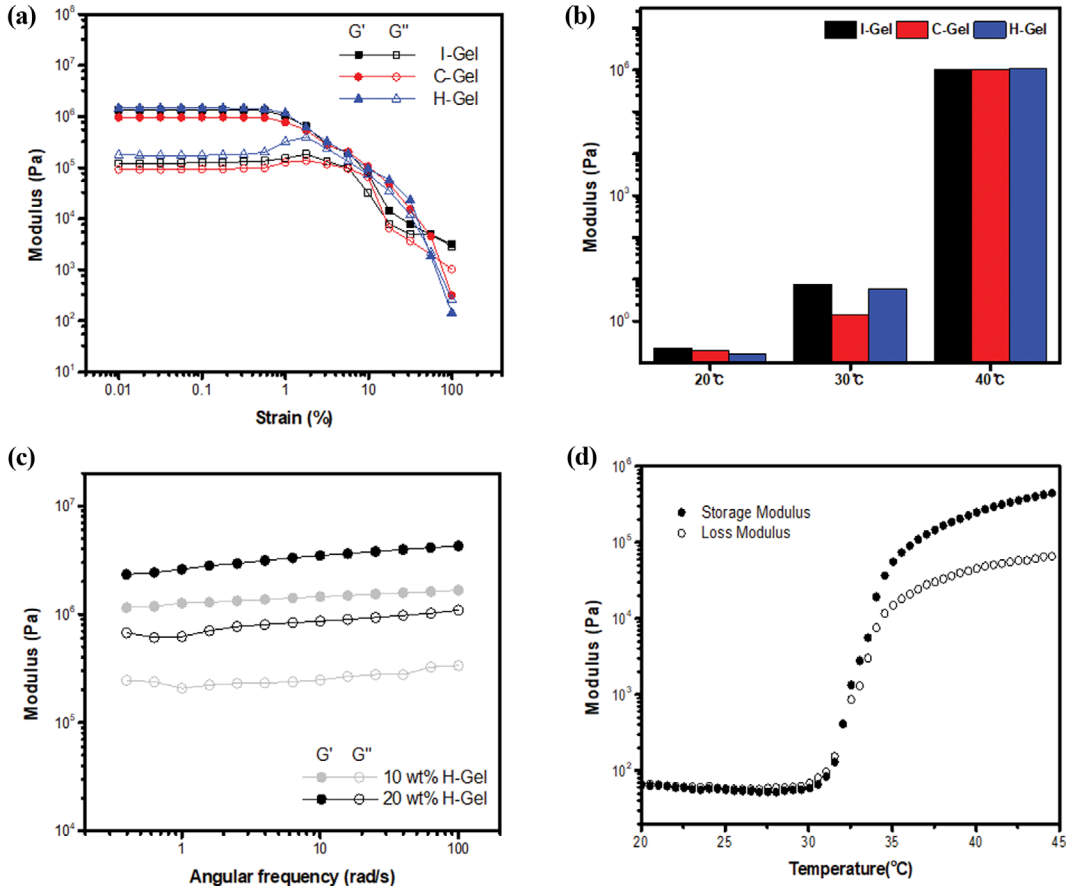

Fig. 7. Rheological properties of $V_{36}C_{36}$kzinc hydrogels (a) Strain sweep measurement result of P-gel, C-gel, and H-gel at 40 °C. (b) The plateau modulus (G_N) of P-gel, C-gel, and H-gel. (c) Frequency sweep measurement result of H-gel at 40 °C. G′ and G″ were measured at two polymer concentrations: 10 (black) and 20 wt% (gray). (d) Temperature sweep measurement result of H-gel. The transition was observed at 32.5 °C, which is CMT.

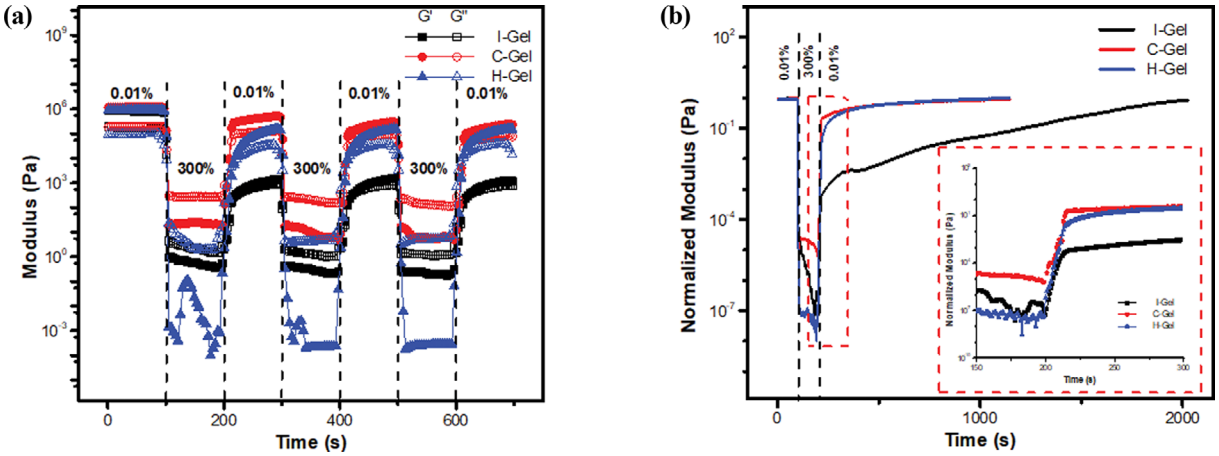

Fig. 8. Recovery Properties of $V_{36}C_{36}$kzinc hydrogels. (a) Cyclic strain measurements up on periodic strain between 0.01% and 300% at 40 °C. (b) Strain jump measurements to determine the time taken for full recovery.

the hydrophobic core of micelle would be deformed due to the weak hydrophobic interaction. Because all hydrogels have the same first cross-linking site, the hydrophobic core, there would be no difference in the deformation of the micelle core. The difference in recovery behavior can be explained by the strength of the second cross-linking. Zn^{2+}-based ionic cross-linking was much weaker than THPC-based covalent cross-linking. At 300% strain, ionic cross-linking would be damaged while covalent cross-linking was not.

Next, the recovery rate was estimated by the strain jump measurement of G′ and G″ (Fig. 8(b)). Time to recover than 99.9% of

G′ in equilibrium showed the difference between hydrogels: 1,800 s for I-gel, 600 s for C-gel, and 800 s for H-gel. Such a difference in the recovery rate was caused by the mechanism of recovery. In the case of C-gel, covalent cross-linking was maintained even at high strain. Thus, only the hydrophobic core of micelles needed to be recovered at low strain, resulting in a quick recovery of C-gel. On the other hand, weak ionic cross-linking of I-gel was damaged at high strain, resulting in a long recovery time. H-gel showed an intermediate behavior because it had both ionic and covalent cross-linking. Thus, we envision that the rate of recovery would be controllable by changing the relative amount of added THPC and zinc ion without affecting G′ and G″ in the equilibrium state.

CONCLUSIONS

We presented ELP-based hydrogel showing thermally induced reversible phase transition and recovery properties. ELPs consist of three blocks: hydrophobic block forming the core of the micelle above the CMT; hydrophilic block located in the corona of the micelle; cross-linking block forming ionic and/or covalent cross-linking depending on the additives. ELP solution was transformed into hydrogel when two conditions were satisfied: 1) the formation of micellular structure at a high temperature; 2) the formation of cross-linking by additives. When one of these requirements was not satisfied, it transformed back into the solution. When all hydrogels were designed to be similar G′ by controlling the cross-linking density, ionic-covalent hybrid gel showed an intermediate recovery rate between slow ionic gel and quick covalent gel. We envision these ELP-based hydrogels be used in a wide range of biomedical applications.

ACKNOWLEDGEMENTS

This work was supported by grants (2018R1D1A1B07041887) and (2021R1A2C2011164) from the National Research Foundation of Korea.

REFERENCES

1. C. Zhang, S. Jin, S. Li, X. Xue, J. Liu, Y. Huang, Y. Jiang, W. Chen, G. Zou and X. J. Liang, *ACS Appl. Mater. Interfaces*, **6**, 5212 (2014).
2. N. Annabi, S. M. Mithieux, G. Camci-Unal, M. R. Dokmeci, A. S. Weiss and A. Khademhosseini, *Biochem. Eng. J.*, **77**, 110 (2013).
3. J. W. Ro, H. Choi, T. Y. Heo, S. H. Choi and J. I. Won, *Biotechnol. Bioprocess Eng.*, **23**, 627 (2018).
4. B. L. LeSavage, N. A. Suhar, C. M. Madl and S. C. Heilshorn, *Jove*, **135**, e57739 (2018).
5. C. Chung, K. J. Lampe and S. C. Heilshorn, *Biomacromolecules*, **13**, 3912 (2012).
6. A. Hennig, G. J. Gabriel, G. N. Tew and S. Matile, *J. Am. Chem. Soc.*, **130**, 10338 (2008).
7. L. Ghasemi-Mobarakeh, M. P. Prabhakaran, M. Morshed, M. H. Nasr-Esfahani and S. Ramakrishna, *Mater. Sci. Eng. C*, **30**, 1129 (2010).
8. D. W. Urry and T. M. Parker, *J. Bioact. Compat. Polym.*, **6**, 263 (1991).
9. Y. N. Zhang, R. K. Avery, Q. Vallmajo-Martin, A. Assmann, A. Vegh, A. Memic, B. D. Olsen, N. Annabi and A. Khademhosseini, *Adv. Funct. Mater.*, **25**, 4814 (2015).
10. L. Li, S. Teller, R. J. Clifton, X. Jia and K. L. Kiick, *Biomacromolecules*, **12**, 2302 (2011).
11. B. A. Cox, B. C. Starcher and D. W. Urry, *J. Biol. Chem.*, **249**, 997 (1974).
12. D. W. Urry, K. Okamoto, R. D. Harris, C. F. Hendrix and M. M. Long, *Biochemistry*, **15**, 4083 (1976).
13. D. W. Urry, *J. Phys. Chem. B*, **101**, 11007 (1997).
14. D. H. T. Le and A. Sugawara-Narutaki, *Mol. Syst. Des. Eng.*, **4**, 545 (2019).
15. J. A. MacKay, D. J. Callahan, K. N. FitzGerald and A. Chilkoti, *Biomacromolecules*, **11**, 2873 (2010).
16. D. E. Meyer and A. Chilkoti, *Biomacromolecules*, **5**, 846 (2004).
17. L. Shi, P. Ding, Y. Wang, Y. Zhang, D. Ossipov and J. Hilborn, *Macromol. Rapid Commun.*, **40**, 1800837 (2019).
18. D. L. Taylor and M. in het Panhuis, *Adv. Mater.*, **28**, 9060 (2016).
19. J. Y. Sun, X. Zhao, W. R. K. Illeperuma, O. Chaudhuri, K. H. Oh, D. J. Mooney, J. J. Vlassak and Z. Suo, *Nature*, **489**, 133 (2012).
20. M. Zhong, Y. T. Liu, X. Y. Liu, F. K. Shi, L. Q. Zhang, M. F. Zhu and X. M. Xie, *Soft Matter*, **12**, 5420 (2016).
21. S. Gu, G. Cheng, T. Yang, X. Ren and G. Gao, *Macromol. Mater. Eng.*, **302**, 1700402 (2017).
22. J. R. McDaniel, J. A. MacKay, F. G. Quiroz and A. Chilkoti, *Biomacromolecules*, **11**, 944 (2010).
23. J. E. Park and J. I. Won, *Biotechnol. Bioprocess Eng.*, **14**, 662 (2009).
24. W. Hassouneh, S. R. MacEwan and A. Chilkoti, *Methods Enzymol.*, **502**, 215 (2012).
25. W. Bode, F. X. Gomis-Ruth and W. Stockler, *FEBS Lett.*, **331**, 134 (1993).
26. E. Hadler-Olsen, B. Fadnes, I. Sylte, L. Uhlin-Hansen and J. O. Winberg, *FEBS J.*, **278**, 28 (2011).
27. A. Vaish, S. G. Roy and P. De, *Polymer*, **58**, 1 (2015).
28. S. M. Janib, M. F. Pastuszka, S. Aluri, Z. Folchman-Wagner, P. Y. Hsueh, P. Shi, Y. A. Lin, H. Cui and J. A. MacKay, *Polym. Chem.*, **5**, 1614 (2014).
29. A. Ghoorchian, J. T. Cole and N. B. Holland, *Macromolecules*, **43**, 4340 (2010).
30. W. Kim, J. Thevenot, E. Ibarboure, S. Lecommandoux and E. L. Chaikof, *Angew. Chem.*, **122**, 4353 (2010).
31. M. Sahn, T. Yildirim, M. Dirauf, C. Weber, P. Sungur, S. Hoeppener and U. S. Schubert, *Macromolecules*, **49**, 7257 (2016).
32. D. Kurkova, J. Kriz, P. Schmidt, J. Dybal, J. C. Rodriguez-Cabello and M. Alonso, *Biomacromolecules*, **4**, 589 (2003).
33. A. Junger, D. Kaufmann, T. Scheibel and R. Weberskirch, *Macromol. Biosci.*, **5**, 494 (2005).
34. C. Xiao, J. Ding, L. Ma, C. Yang, X. Zhuang and X. Chen, *Polym. Chem.*, **6**, 738 (2015).
35. E. Meco and K. J. Lampe, *Biomacromolecules*, **20**, 1914 (2019).
36. S. Sun and P. Wu, *Macromolecules*, **46**, 236 (2013).
37. J. Spevacek, J. Dybal, L. Starovoytova, A. Zhigunov and Z. Sedlakova, *Soft Matter*, **8**, 6110 (2012).
38. G. Le Fer, A. L. Wirotius, A. Brulet, E. Garanger and S. Lecommandoux, *Biomacromolecules*, **20**, 254 (2018).
39. Q. Li, D. G. Barrett, P. B. Messersmith and N. Holten-Andersen, *ACS Nano*, **10**, 1317 (2016).